ML Surrogate for a CAD Model - Application to the Shape Optimization of the DLR-F25 Transport Aircraft

M G Kontou[1], **V G Asouti**[1,2], **X S Trompoukis**[1,2] **and K C Giannakoglou**[1]
[1]Parallel CFD & Optimization Unit, School of Mechanical Engineering, National Technical University of Athens, Athens, Greece
[2]FOSS: Flow & Optimization, Software & Services, Piraeus, Greece

Keywords: Machine Learning, Deep Neural Networks, Aerostructural Shape Optimization, CAD Model, Continuous Adjoint

Abstract. This paper demonstrates the development and use of Machine Learning (ML) models to replace critical CAD-related parts in a gradient-based shape optimization (ShpO) workflow, as for instance in the aerodynamic or aerostructural optimization of an aircraft. To this end, Deep Neural Networks (DNNs), in the form of the two-branch λ-DNN architecture developed by the group of authors in previous works, replace the CAD-based parameterization of the aircraft wing shape. The λ-DNN is trained on a set of snapshots (point clouds) of the aircraft surface for various design variable sets. It is used in the deformation of the wing, without having access to the corresponding CAD model. Inputs to the λ-DNN are the nodal coordinates of the baseline geometry and the design vector of each new geometry. The required sensitivities of surface coordinates with respect to CAD parameters are computed by differentiating the λ-DNN. The ML models support the in-house GPU-enabled flow solver PUMA and a structural analysis code, both with their adjoints. The optimization workflow is used to optimize the high-aspect-ratio wing of the DLR-F25 transport aircraft, for minimum drag, under lift and pitching moment constraints. Single-point optimization studies, both aerodynamic and aerostructural, are presented.

1. Introduction

ML models are nowadays indispensable parts of Computational Fluid Dynamics (CFD)-based optimization. About two or three decades ago, Artificial Intelligence (AI) tools found their own way in stochastic population-based optimization [1,2]. Their role was to speed up the design process by replacing repetitive calls to computationally expensive analysis tools. Nowadays, ML tools are also used for the same purpose; for instance, in [3], the ML model is trained on a database of wing-planforms and used within a multi-objective genetic algorithm to optimize the wing of the NASA Common Research Model; or, [4] presents a deep learning-based framework that automates the generation and evaluation of 3D CAD designs in the conceptual design phase of engineering components such as car wheels.

In real world engineering problems, shape optimization (ShpO) typically starts from a CAD-generated geometry and tries to deliver the optimized shape in the same CAD format. To do so, one should either incorporate the CAD model into the optimization loop, [5], which has a lot of issues, or re-generate the CAD model anew, by fitting it to the optimized shape, which is prone to performance loss.

The λ-DNN architecture, initially proposed by the group of authors as surrogate for turbulence and transition closure in CFD, [6,7], is herein used to replace a CAD-based parameterization within a real-world ShpO loop. The λ-DNN recomputes a point cloud on a patch of the aircraft surface (including the wing and the wing-to-fuselage fairing), each time the values of the CAD model parameters, used to generate the initial shape, change during the optimization. It is also differentiated to compute mesh sensitivities, i.e. the gradients of the surface nodal coordinates with respect to (w.r.t.) the CAD parameters/design variables. This ML model is incorporated into an adjoint-based aerodynamic/ aerostructural optimization loop built around the NTUA CFD code PUMA, a Computational Structural Model (CSM) code and their adjoints; the CAD model is absent from the loop. This workflow is used for the design/optimization of the next-generation high aspect-ratio wing DLR-F25 transport aircraft, studied in the framework of the EU funded project NEXTAIR.

2. Aerostructural shape optimization tools

A gradient-based aerostructural ShpO loop for aircraft applications traditionally involves CFD and CSM tools as well as their adjoints. The corresponding aerostructural workflow, split into two parts, is shown in figure 1. On the left, the analysis or primal loop is presented, by omitting though convergence criteria. It includes the CFD and CSM analysis, as well as the linking blocks, i.e. load transfer from CFD to CSM, transfer of deformations in the opposite direction, as well as the process for adapting the CFD mesh to new surface meshes using an in-house two-step radial basis function (RBF)-based tool [8]. In each optimization cycle, upon convergence of the aforesaid analysis loop, the adjoint loop (shown on the right) follows; this involves the adjoint CFD and CSM codes as well as the adjoint load and adjoint deformation transfers. What is missing from figure 1 is the optimization loop that coordinates the primal and adjoint solvers, with extra boxes accounting for the computation of the gradient of the objective and constraint functions, the update of the design (CAD) variables and the update of the geometry in each optimization cycle. If the CAD model was on board, the CAD parameter values would directly be updated, provided that the derivatives of the surface coordinates w.r.t. the CAD parameters were available. However, in the application(s) presented in this paper, the CAD model was not available and, even if this was not the case, our intention is to avoid bringing the CAD model into the optimization loop.

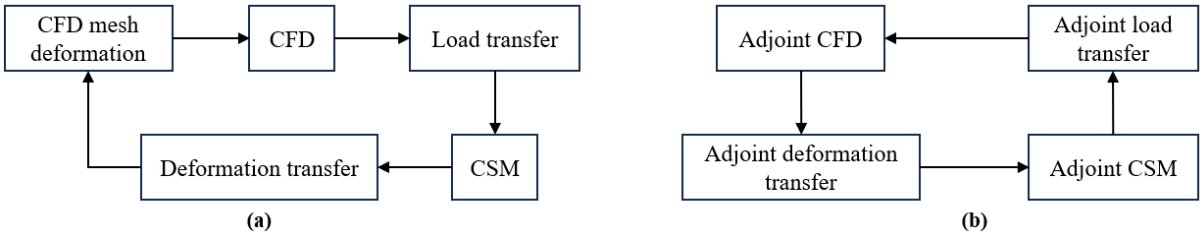

Figure 1. Schematic representation of the CFD-CSM primal (a) and adjoint (b) workflow of the optimization loop.

In the present studies, the PCOpt/NTUA GPU-enabled code PUMA, [9], is used for the CFD analysis. It solves the RANS equations on unstructured/hybrid meshes using vertex-centered finite volumes. It also involves a continuous adjoint method, that makes use of consistent discretization schemes for the adjoint equations to enjoy high accuracy in the computed sensitivity derivatives, without losing the physical insight into the adjoint problem [10]. For the CSM analysis, MSC Nastran is utilized alongside a structural model provided by DLR. The latter is initially built based on conceptual design loads and, then, sized through an iterative process. This process involves: (a) the identification of critical load cases by conducting aeroelastic analyses for multiple load scenarios covering the whole flight envelope, and (b) the optimization of the thickness distribution of shell elements based on these critical load cases, both based on MSC Nastran. A detailed description of the PUMA flow and adjoint solvers as well as the coupling with a CSM code and its adjoint can be found in [11]. Below, the involvement of the ML model into the aerostructural workflow is presented in more detail.

On the other hand, the λ-DNN architecture [7] is based on fully connected neural networks with two input branches (likely with a different number of layers each) that merge into a main (output) branch, which further processes signals through its layers and produces the network's outputs. This architecture, that resembles the Greek letter λ (hence, the name λ-DNN), is beneficial due to the separate processing of input data of different type, leading to the extraction of distinctive features from each branch before merging them into the final output. Here, the first input branch processes the coordinates of the baseline geometry (in the form of cloud point, i.e. surface nodes different from those of the CFD mesh) and the second one the design (CAD) variables vector, the deformations of which are computed at the output branch, figure 2. To generate the K training samples of the λ-DNN, access to a CAD model is required to generate a set of P nodes (point cloud) on the surface of the geometry corresponding to any value-set

of the N design variables. To further increase the accuracy and reliability of the networks, it is highly recommended to optimize their configuration; this is carried out by means of metamodel-assisted evolutionary algorithms [6]. The optimizations aimed to decrease the prediction error of the networks by defining the best combination of a number of layers per branch, number of neurons per layer and activation functions. The λ-DNN was also differentiated and used in the gradient-based aerostructural ShpO. For the former, the derivatives of the geometrical surface deformations w.r.t. the design variables are computed using automatic differentiation.

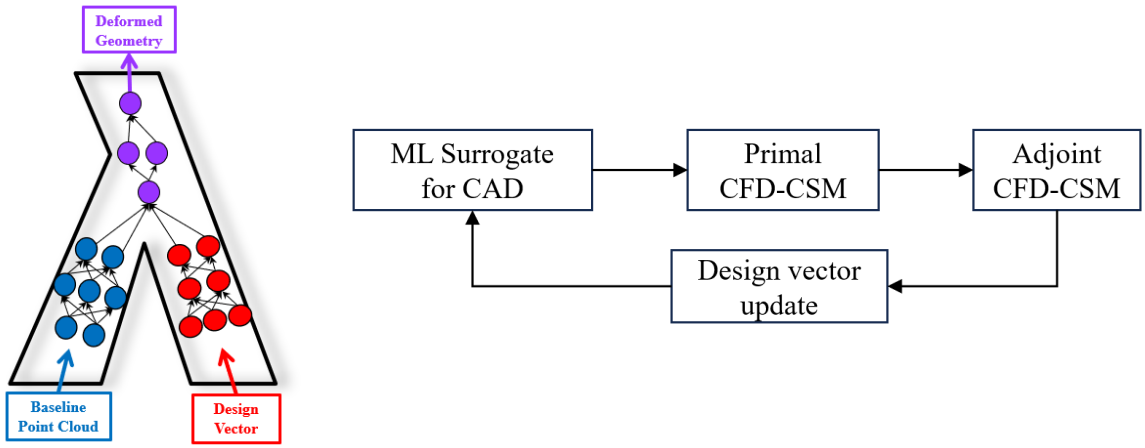

Figure 2. The λ-DNN architecture (left) and the aerostructural optimization workflow (right) supported by the ML model.

3. Applications – Discussion

The previously described tools were used for the ShpO of the wing of the DLR-F25 aircraft. The λ-DNN was used to replace the aircraft parametric CAD of DLR (generated using CATIA V5R28) that was not accessible to NTUA. During the ShpO, only the wing shape can change, and the design variables amount to N=8x6+5=53 CAD parameters associated with the wing: the camber at 6 spanwise sections are controlled by one octet of variables each, and 5 more variables control the twist angles at 5 (out of these 6) sections. Using different combinations of the values of the N design variables, K=1992 aircraft shapes with P=7080 nodes each, located over the wing and the wing-to-fuselage fairing (figure 3a) were generated. 1972 out of the K shapes were used for training the λ-DNN, and 20 (plus the baseline; 21, in total) for testing.

Three networks have been trained by separately processing the x, y, or z coordinates of the baseline point cloud on the left branch and predicting the corresponding deformations at the output. Various tests showed that introducing the baseline surface coordinates as an extra input increased the accuracy and smoothness of predictions, as this acts as an extra bias, further processed by the output branch. All networks have optimized configurations as in table 1. Training the so-optimized configurations and

using the λ-DNNs yield a prediction error of ~$7.8 \cdot 10^{-4}$ m (for the 21 testing samples). The prediction error fields, for a new wing (not seen by the networks), are presented in figure 3b.

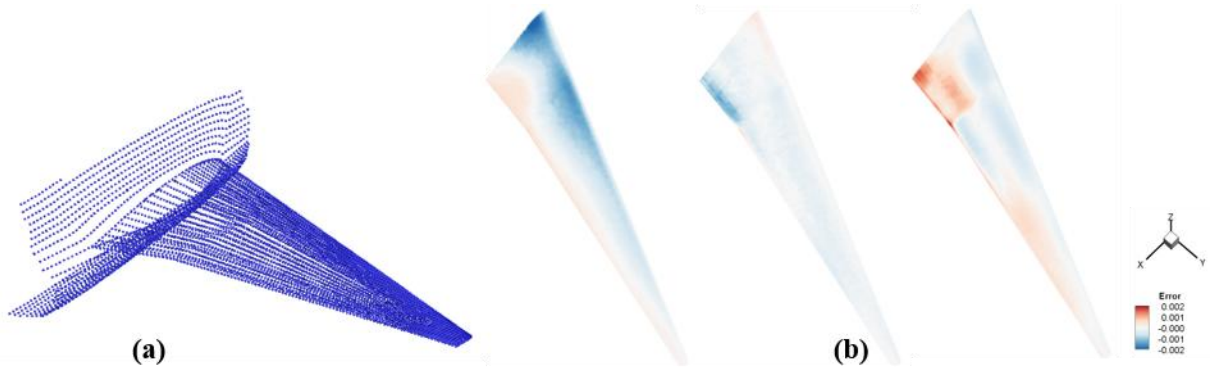

Figure 3. (a) Point cloud of the baseline aircraft geometry processed by the left input branch of the λ-DNN. (b) Prediction error of the λ-DNNs at the x, y and z directions.

Table 1. Optimized λ-DNN architectures used to replace the CAD model.

		Layers	Neurons/Layer	Act. Functions
x-coordinate	Left input branch	4	128/2048/1024/256	*tanh*
	Right input branch	4	128/1024/2048/256	*tanh*
	Output branch	3	64/128/256	sigmoid
y-coordinate	Left input branch	5	1024/128/64/256/64	GELU
	Right input branch	4	128/2048/2048/64	GELU
	Output branch	1	256	sigmoid
z-coordinate	Left input branch	5	32/128/64/64/2048	GELU
	Right input branch	3	256/4096/2048	sigmoid
	Output branch	2	256/1024	sigmoid

The new optimization workflow was used for the aerodynamic (rigid wing) and aerostructural ShpO runs, both at cruise conditions (altitude 36000ft and M_∞=0.78). The flow is turbulent and the adjoint to the turbulence model equation (herein the Spalart-Allmaras) was included into the optimization runs. In either case, the optimization aimed at minimizing the drag coefficient (C_D) while keeping the aircraft trimmed (C_M=0; practically $|C_M|<10^{-4}$) and the lift coefficient equal to that at cruise ($|C_L-0.59|<10^{-4}$). Regarding C_M, the Horizontal Tail Plane (HTP) angle was adapted to yield a trimmed aircraft during each aerodynamic or aerostructural optimization cycle. The convergence histories of the objective and constraint functions are given in figures 4a and 4b for the two ShpO runs. A decrease in C_D by ~8% (aerodynamic ShpO) and ~5.5% (aerostructural ShpO) respectively, was obtained, while meeting all the imposed constraints. The pressure coefficient fields on the wing surface for the baseline and the optimized aircraft are presented in figures 5 and 6. The strong shock wave over the wing that appears on the baseline configuration is suppressed in the optimized ones.

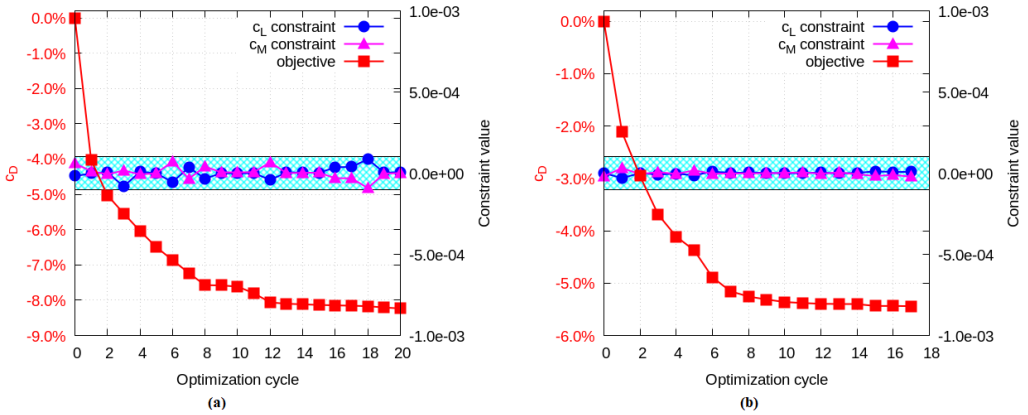

Figure 4. Evolution of the objective and constraint functions for the aerodynamic (a) and the aerostructural (b) optimization runs.

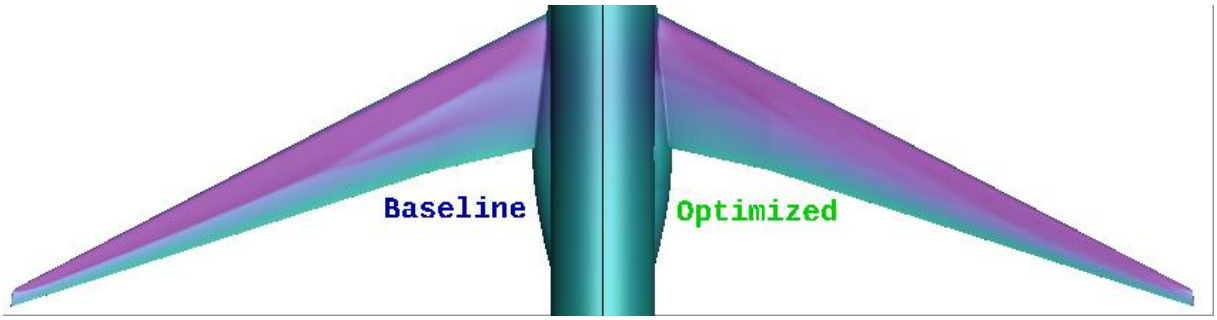

Figure 5. Aerodynamic ShpO: Pressure coefficient fields computed on the wing suction side for the baseline (left) and the optimized (right) geometries.

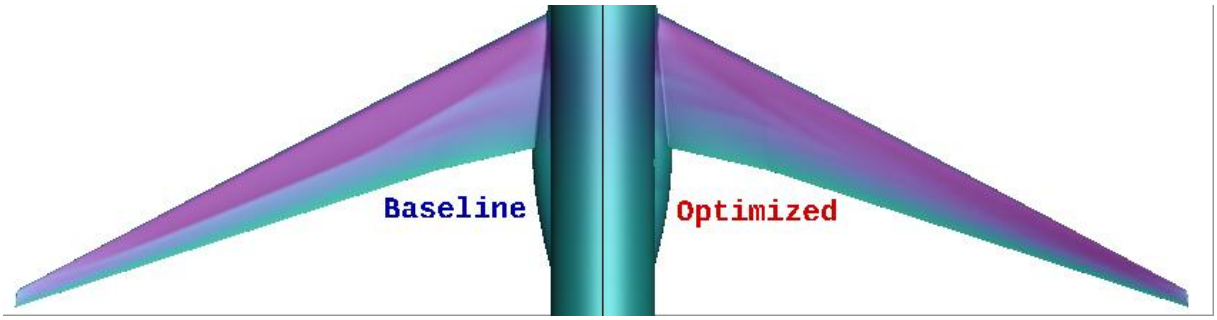

Figure 6. Aerostructural ShpO: Pressure coefficient fields computed on the wing suction side for the baseline (left) and the optimized (right) geometries.

The airfoil profiles at different spanwise locations are shown in figure 7. Close to the root, the two optimizations resulted in similar airfoil profiles. Major differences appear only close to the tip where the elastic effects are pronounced. In the rigid case, the wing gets a negative twist and the wing tip is significantly twisted. The aerostructurally optimized wing, at the tip, is slightly cambered close to the trailing edge and untwisted (see figure 6e). This behavior, combined with the increase in the AoA which is necessary to meet the lift constraint, leads to higher wing bending and twist.

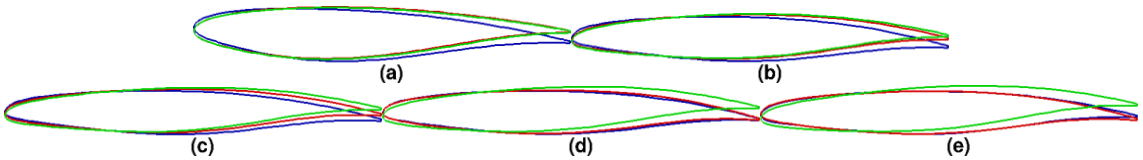

Figure 7. Airfoil profiles at different spanwise cross-sections (18%, 35%, 50%, 70%, 90%) for the baseline (blue), the aerodynamically (green) and the aerostructurally optimized (red) wings.

4. Conclusions

It was demonstrated that ML models, in the form of properly trained λ-DNNs, can successfully be used to replace the CAD model into aerodynamic and aerostructural ShpO loops. By training on point clouds and integrating with adjoint solvers, the models enabled efficient gradient-based optimization without direct access to the CAD model. Their high prediction accuracy was demonstrated not only by their exceedingly small prediction error, but also by their contribution on the computation of the required gradients.

Acknowledgments

This work is part of the NEXTAIR project which is funded by the European Union (GA number 101056732). Views and opinions expressed are those of the author(s) only and do not necessarily reflect those of the European Union or REA. Neither the European Union nor the REA can be held responsible for them. DLR-F25 was developed within the German Federal Aviation Research Programme (LuFo), funded by the German Federal Ministry for Economic Affairs and Climate Action (BMWK).

5. References

[1] K. Giannakoglou 'Design of optimal aerodynamic shapes using stochastic optimization methods and computational intelligence', Prog Aerosp Sci., 38:43-76, 2002. https://doi.org/10.1016/S0376-0421(01)00019-7

[2] Y. Jin 'Surrogate-assisted evolutionary computation: Recent advances and future challenges', Swarm Evolv Comput, 1:61-70, 2011. https://doi.org/10.1016/j.swevo.2011.05.001

[3] M. Hasan, S. Redonnet, D. Zhongmin 'Aerodynamic optimization of aircraft wings using machine learning', Adv Eng Softw, 200:103801, 2025. https://doi.org/10.1016/j.advengsoft.2024.103801

[4] S. Yoo, S. Lee, S. Kim, K.-H. Hwang, J, Park, N. Kang 'Integrating deep learning into CAD/CAE system: generative design and evaluation of 3D conceptual wheel', SAMO, 2021, https://doi.org/10.1007/s00158-021-02953-9

[5] T. Robinson, C. Armstrong, H. Chua, C. Othmer, T. Grahs 'Optimizing parameterized CAD geometries using sensitivities based on adjoint functions', Comput Aided Des, 9:253-268, 2013, https://doi.org/10.3722/cadaps.2012.253-268

[6] M. Kontou, V. Asouti, K. Giannakoglou 'DNN surrogates for turbulence closure in CFD-based shape optimization', Appl Soft Comput, 134:110013, 2023, https://doi.org/10.1016/j.asoc.2023.110013

[7] M. Kontou, D. Kapsoulis, I. Baklagis, X. Trompoukis, K.C. Giannakoglou 'λ-DNNs and their Implementation in Conjugate Heat Transfer Shape Optimization', Neural Comput Appl, 34:843-854, 2022, https://doi.org/10.1007/s00521-021-05858-2

[8] F. Gagliardi, K. Giannakoglou 'A Two-Step Radial Basis Function-Based CFD Mesh Displacement Tool', Adv. Eng. Softw., 128:86-97, 2019, https://doi.org/10.1016/j.advengsoft.2018.11.011

[9] V. Asouti, X. Trompoukis, I. Kampolis, K. Giannakoglou 'Unsteady CFD computations using vertex-centered finite volumes for unstructured grids on Graphics Processing Units', Int J Numer Methods Fluids, 67:232-246, 2011, https://doi.org/10.1002/fld.2352.419

[10] K. Giannakoglou, V. Asouti, E. Papoutsis-Kiachagias, N. Galanos, M. Kontou, X. Trompoukis 'The Think Discrete-Do Continuous Adjoint in Aerodynamic Shape Optimization', EUROGEN 2023, 15th International Conference on Evolutionary and Deterministic Methods for Design, Optimization and Control, Chania, Crete, Greece, 1-3 June 2023, http://dx.doi.org/10.7712/140123.10201.18965

[11] K. Tsiakas, X. Trompoukis, V. Asouti, K. Giannakoglou, G. Rogé, S. Julisson, L. Martin, S. Kleinveld 'Continuous Adjoint-Based Aerostructural Wing Shape Optimization of a Business Jet', Fluids, 9:87, 2024, https://doi.org/10.3390/fluids9040087